Numerical studies of MHD equilibrium and stability with bootstrap current in the CFQS quasi-axisymmetric stellarator

X. Q. Wang[1], Y. Xu[1], A. Shimizu[2], M. Isobe[2,3], S. Okamura[2], Y. Todo[2], H. Wang[2], H. F. Liu[1], J. Huang[1], X. Zhang[1], H. Liu[1], J. Cheng[1], C. J. Tang[4] and the CFQS term

1 Institute of Fusion Science, School of Physical Science and Technology Southwest Jiaotong University, Chengdu 610031, China

2 National Institute for Fusion Science, National Institutes of Natural Sciences, Toki, Gifu 509-5292, Japan

3 SOKENDAI (The Graduate University for Advanced Studies), Toki, Gifu 509-5292, Japan

4 School of Physical Science and Technology, Sichuan University, Chengdu 610041, China

In this paper, typical configurations of the Chinese first quasi-axisymmetric stellarator (CFQS) are calculated by the HINT code [1]. In the quasi-axisymmetric magnetic configuration of the CFQS, a substantial bootstrap current can be present in the high-β regime [2,3]. Therefore, the equilibrium including bootstrap currents should be calculated in order to explore the configuration properties. In this work, the bootstrap current was estimated using the BOOTSJ code based on the drift kinetic model. The calculations were iterated many times until the BOOTSJ calculation based on the equilibrium with bootstrap currents result in the same bootstrap current profile so that the final bootstrap current profiles and amplitudes are convergent.

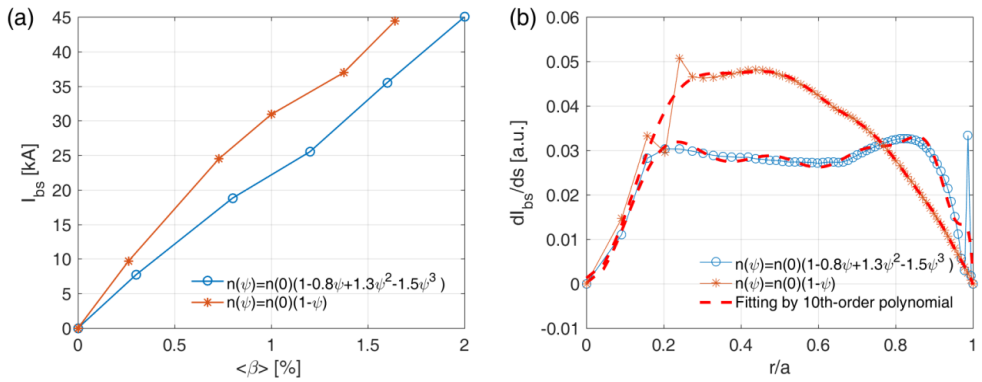

Figure 1. (a) Bootstrap current (I_{bs}) as a function of <β> and (b) radial profile of the bootstrap current density (dI_{bs}/ds) at <β>≈1% for the parabolic density profile (Case 1) and the flat density profile (Case 2) calculated by the BOOTSJ code. The dashed lines in figure 4(b) are the best fitting of the 10th-order polynomial.

To study the effects of the bootstrap current, we consider two cases of the density profile, i. e., Case 1: the parabolic density profile $n(\psi) = n(0)\cdot(1-\psi)$ and Case 2: the flat density profile $n(\psi) = n(0)\cdot(1-0.8\psi+1.3\psi^2-1.5\psi^3)$. In this work, in order to focus on the profile effect, the central electron and ion densities on the axis are fixed as $n_e(0)=n_i(0)=10^{19}\,m^{-3}$. The electron and ion temperature profiles are $T_e(\psi) =T_e(0)\cdot(1-\psi)$ and $T_i(\psi) = T_i(0)\cdot(1-\psi)$ with $T_i(0) = 0.75T_e(0)$. The central values of the temperature depend on central plasma beta (or pressure) values. For example, in figure 1 for a central beta value β_0=2.5% with B_t=1.0T, $T_e(0)$ = 3.55 keV and $T_i(0)$ = 2.66 keV. From figures 1(a) and (b), we can see that a flat density profile can effectively reduce the amplitude of bootstrap currents and change the current density profile significantly. For the present CFQS design of $<\beta>\sim$1%, the amplitude of the bootstrap current (I_{bs}) is about 30kA and 20 kA for Case 1 and Case 2, respectively. It is interesting to note that in Case 1, the profile of the bootstrap current density (dI_{bs}/ds) has a peak in the range of $r/a \approx$(0.3-0.6), which may result in a reversed magnetic shear in the bulk plasma, whereas in Case 2 the flat profile of dI_{bs}/ds in the central region suggests a locally weak magnetic shear. It has to be pointed out that the spikes in the current profiles occur when the rotational transform crosses low-order rational surfaces.

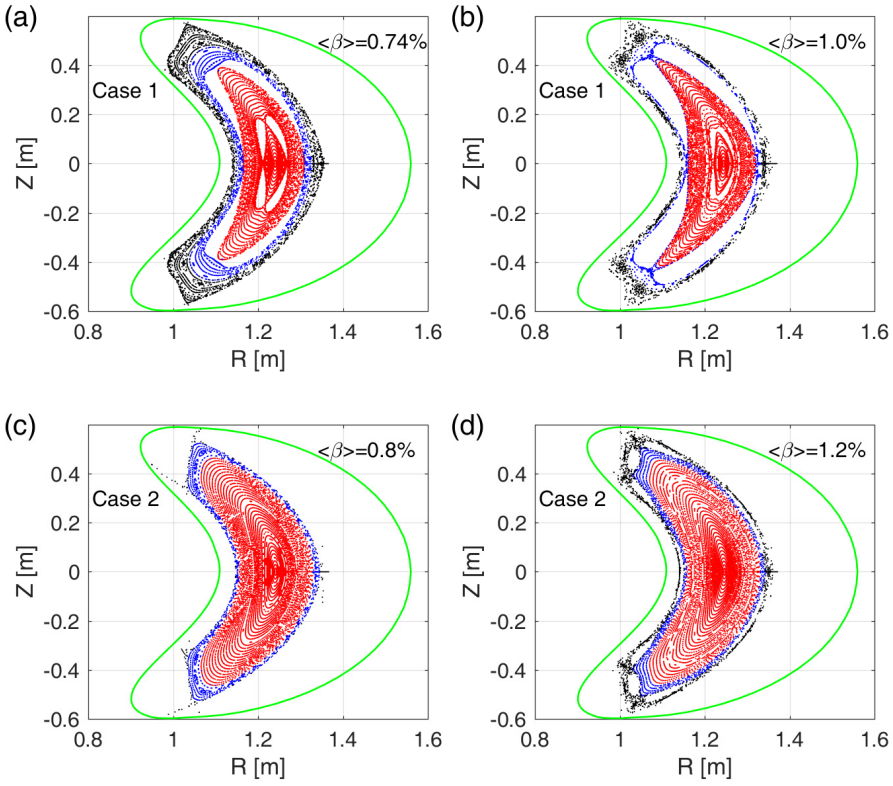

Figure 2. Poincaré plots of magnetic surfaces for (a-b) Case 1 and (c-d) Case 2 at different <β> values, where the black, blue and red colours mark the regions of $p/p_0<1\%$, $1\%\leq p/p_0\leq 10\%$, and $p/p_0>10\%$, respectively. The green line denotes the boundary of the vacuum vessel.

To further survey the properties of islands in QAS, we have calculated the equilibria of the CFQS with the bootstrap current by the HINT code. The Poincaré plots of magnetic surfaces are depicted in figure 2 for the Case 1 and 2, where the black, blue and red colours mark the region of $p/p_0<1\%$, $1\%\leq p/p_0\leq 10\%$, and $p/p_0>10\%$, respectively. For Case 1, figures 2(a) and (b) show that with increasing beta from 0.74% to 1% the widths of the 2/4-island and 4/9-island chains both increase so that the space between these two island chains becomes smaller. Thus, the island chains connected to intermediate rationals, particular 6/13 and 8/17 islands grow as well and their overlap contributes to the generation of the stochastic region between the 4/9- and 2/4-islands. For Case 2, as shown in figures 2(c) and (d), the magnetic islands and the field line stochastization are remarkably suppressed in comparison with Case 1. In such a scenario the iota-profiles do not contain the $\iota/2\pi=2/4$ resonance, and hence, a 2/4-island cannot appear in the magnetic topology of the field. Although the boundary 4/9-island chain remains, the good flux surfaces are still kept over the entire plasma area. Furthermore, the 4/9-island chains in Case 1 and Case 2 exhibit different island phases, which is possibly due to different distributions of equilibrium currents and net-currents in the two calculations. These results offer a possible prediction for the high-β equilibrium of the CFQS and suggest that the high-β operation scenarios can be realized if density profiles can be controlled by the electron cyclotron resonance heating, pellet injection and so on. Besides, a change in the temperature profiles may also serve the same goal.

The study of MHD instabilities is essential to evaluate the basic properties of QAS configurations, in particular, the ideal instabilities including the kink and ballooning modes, have drawn close attention in the physical design and optimization of the QAS. As an initial value MHD code, MEGA code is a powerful tool to study nonlinear MHD instabilities in 3D tokamaks and stellarators [4]. Therefore, in this work, simulations of global MHD stabilities have been carried out by the MEGA code for Case 2 and the equilibrium configurations calculated in section 2 with $<\beta>=1.2\%$ are used. In the simulation, the potential MHD instabilities are considered self-consistently by adopting an initial random perturbation. The plasma viscosity and diffusion coefficients are set to be 10^{-5} to maintain the numerical stability. The plasma resistivity, η, is taken to be 5×10^{-5} (unless stated in other specific cases). The growth rate and frequency of the modes are normalized by the Alfvén frequency(ω_A) in the equilibrium of Case 2 in which the Alfvén time is $\sim1.4\times10^{-7}$ s with the plasma density being 1×10^{19} m^{-3}. A Boozer coordinate system of the equilibrium was constructed for the spectral analysis of the simulation results.

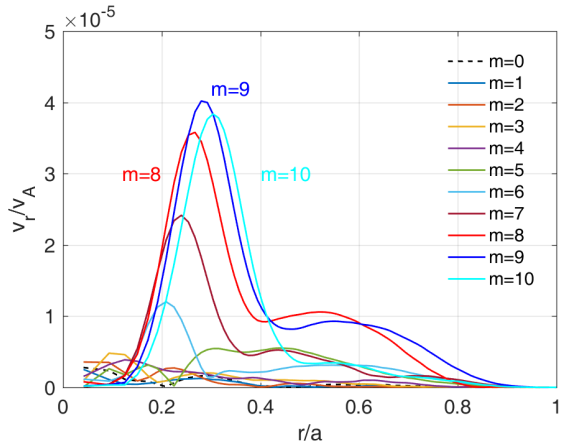

Figure 3. The radial profiles of the normalized radial velocity for m=0~10 and n=−4.

The radial eigenmode structures of the unstable modes with the dominant toroidal mode number n=−4 and the poloidal mode number m=0~10 are shown in figure 3, where the radial velocity (v_r) is normalized to the Alfvén velocity v_A. The dominant mode numbers (n=−4 and m=8, 9 and 10) are related to the rational values 4/8 (=1/2), 4/9 and 4/10 (=2/5). The peaking locations are all near the rational surface of 1/2 and also close to the weak shear regions. It is clear that the radial structure shows a strong mode coupling around the same location.

Acknowledgments

The authors would like to thank Prof. Y. Suzuki for his great help on using the HINT code for the CFQS.

References

[1] Suzuki Y. *et al* 2006 *Nucl. Fusion* 46 L19

[2] Shimizu A. et al 2018 Plasma Fusion Res. 13 3403123

[3] Liu H. F. et al 2018 Plasma Fusion Res. 13 3405067

[4] Todo Y. *et al* 1998 *Phys. Plasmas* 5 1321